Available online at www.sciencedirect.com
ScienceDirect
Acta Biomaterialia 4 (2008) 131–138
Acta BIOMATERIALIA
www.elsevier.com/locate/actabiomat

The growth of nacre in the abalone shell

Albert Yu-Min Lin *, Po-Yu Chen, Marc André Meyers

Department of Mechanical and Aerospace Engineering, Materials Science and Engineering Program, University of California, San Diego, La Jolla, CA 92093-0411, USA

Received 11 January 2007; received in revised form 16 April 2007; accepted 2 May 2007
Available online 9 July 2007

Abstract

The process of mineral formation following periods of growth interruption (growth bands) is described. Flat pearl implantation as well as a new trepanning method are used to observe the transitory phases of calcium carbonate which nucleate and grow during this process. An initial random nucleation of the aragonite polymorph is observed followed by a transition towards spherulitic growth. During this transition the animal forms the structure of the shell through both mechanical and chemical actions. About 6 weeks after implantation a steady-state growth of aragonite tiles begins after shorter and more irregular tiles cover the outer surface of the spherulites. The growth rate of aragonitic spherulite during this transition period was calculated to be approximately 0.5 μm per day. An organic scaffolding is observed during the steady-state growth of tiled aragonite. Observations of mineral growth following the deposition of these membranes confirm the presence of mineral bridges originating from subsurface tiles and extending through the organic matrix, confirming the growth model proposed by Schäffer et al. [Schäffer TE, Ionescu-Zanetti C, Proksch R, Fritz M, Walters, DA, Almqvist N, et al. Does abalone nacre form by heteroepitaxial nucleation or by growth through mineral bridges? Chem Mater 1997;9:1731–40]. Field emission scanning electron microscopy of fractured deproteinated nacre shows the presence of mineral bridges existing between individual layers of tiles. Transmission electron microscopy provides further evidence of mineral bridges.

Keywords: Abalone; Nacre; Biomimetics; Self-assembly; Biological materials

1. Introduction

Crystallization of inorganic materials in nature generally occurs at ambient temperature and pressure. Yet the simple organisms through which these inorganic materials form are able to create extremely precise and complex structures. Understanding the process in which living organisms control the growth of structured inorganic materials could lead to significant advances in materials science, opening the door to novel synthesis techniques for nanoscale composites [1–4].

The nacre from the shell of the abalone (*Haliotis*) has become one of the more intensively studied biological structures in materials science. The highly ordered microscale aragonite tiles separated by thin nanoscale organic sheets along with a macrostructure of larger periodic growth bands form a hierarchical composite [5]. Early work by Jackson et al. [6] and Currey [5] showed that the overall composite consists of only 5 wt.% organic material, yet the work to fracture was increased by up to ~3000 times over inorganic $CaCO_3$ crystals as a result of the intricate hierarchy of structural organization. Other studies have shown impressive results (an eight-fold increase) for the fracture toughness; similarly, the tensile strength is increased significantly [7–11].

The process of biomineralization by which these shells form involves the selective identification and uptake of elements and ionic molecules from the local environment and their incorporation into structures under strict biological mediation and control [12–16]. It is possible (and indeed probable) that organic mediation accelerates the mineralization process. This is presented by Mann [14]. The formation

* Corresponding author. Tel.: +1 858 534 4719.
E-mail address: a5lin@ucsd.edu (A.Y.-M. Lin).

1742-7061/$ - see front matter © 2007 Acta Materialia Inc. Published by Elsevier Ltd. All rights reserved.
doi:10.1016/j.actbio.2007.05.005

and deposition of steady-state nacre has been given considerable attention in recent years. However, less work has been done to examine the development of periodic growth bands which exist throughout the shell. This study intends to reveal the process of mineralization following these periods of growth interruption.

2. Experimental methods

Both the "flat pearl" technique, pioneered by the UC Santa Barbara group (e.g. [17]), and a new "trepanning" technique were used to observe the various formations following steady-state growth interruption. Substrates were implanted in live red abalone (*Haliotis rufescens*) for periods of 1–6 weeks and subsequently extracted weekly for immediate observation. Adult-sized animals were collected from both the culturing facility, Marine Bioculture in Leucadia, CA, and their natural environment off the coast of southern California, and then held in an open water facility at the Scripps Institution of Oceanography. Constant circulation of fresh seawater provided a natural environment with steady pH and realistic temperature fluctuations around a mean temperature of approximately 16 °C. The holding tanks were curtained, limiting the exposure to exterior lighting, creating a similar ambiance to the natural habitat of both red and green abalone. All animals were fed giant kelp (*Macrocystis pyrifera*) on a regular schedule.

Circular glass slides 15 mm in diameter were glued onto the growth surface of adult-sized abalone. This surface was exposed by gently pushing back the mantle layer in the inside of the shell using a flat stainless steel scalpel with round, dull edges. Up to six slides were implanted in each animal. The epithelial layer of skin (mantle) repositioned itself over the implanted glass slides over a period of a few days. Slides were then extracted from the living animals on a weekly basis and prepared for immediate SEM observation by applying a thin gold–palladium plating. Unlike our previous experiments [8], the samples were not rinsed with purified water before examination.

A second experiment was carried out simultaneously in which a foreign substrate of abalone nacre was polished, destroying its original growth surface, and implanted onto the growth surface of a live abalone. Pucks of nacre, 3 mm in diameter, were drilled from these shells using a diamond coring drill. Holes slightly larger than 3 mm were then drilled in the shells of live abalone, allowing a press fit of the pucks into designated positions along the growth surface. During this process the drilled area was continuously irrigated and cooled with chilled seawater. This method of trepanning provided a natural substrate on which growth could restart. Although the implant surfaces were polished, the surface activation energy of the implant and host nacre is similar, being that they are the same material. The pucks were then left for periods of 1–6 weeks before being removed simultaneously with the above-mentioned flat pearls. Fig. 1 shows both the flat pearl and the trepanning techniques on the shell of an abalone.

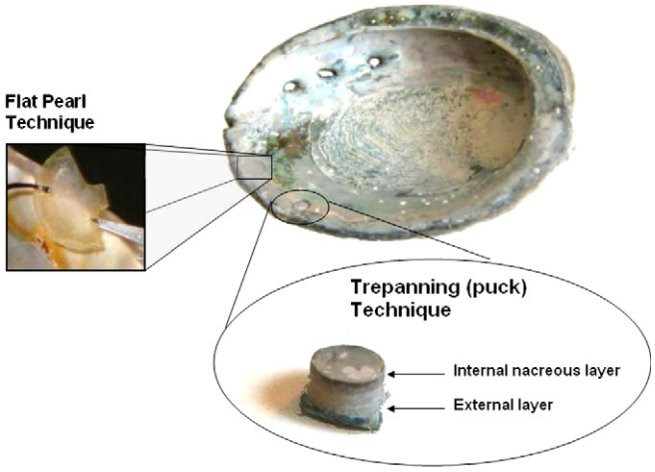

Fig. 1. Implantation methods: trepanning and flat pearl.

Specimens were removed from animal growth surfaces for a period of less than 1 h before examination with a FEI XL30 field emission scanning electron microscope (SEM), with electron diffraction spectroscopy (EDS). SEM samples were transported to the characterization facilities in a bath of chilled seawater, and air dried for 5 min prior to gold plating.

A Renishaw Raman spectrometer was used to determine the composition of the biomineralized material. Samples which were not gold plated were placed under a 514.4 nm wavelength laser with a beam energy of 1 mW.

To observe mineral bridges between individual tiles, nacre was fractured in tension parallel to the direction of growth. Cylindrical pucks with 3 mm diameters were drilled from fresh nacre and glued onto tensile testing platents using J–B weld epoxy resin and left to cure for 24 h. After fracture by tension, a common deproteination technique was applied to remove the organic component of the shell [18]. The fracture surface was immersed directly into 10 ml of hydrazine (98.5%) at room temperature for periods of 1, 2 and 9 h to remove the organic component of the tiled structure. The samples were then serially diluted with absolute ethanol under 5 min increments of increasing concentrations of ethanol at 50%, 75%, 87.5% and then 100%. After air drying, the samples were gold plated and observed by SEM.

Transmission electron microscopy was conducted on nacre perpendicular to the direction of growth. Thin slices of nacre were sectioned using a high-speed diamond saw, then ground into 3 mm diameter slides by hand. They were mechanically dimpled to a minimum thickness of 100 μm before ion milling and then polished to perforation using an ion mill with a voltage of 5.5 kV and a current of 0.5 mA. Observations were made using a FEI 200 kV Sphera microscope.

3. Results and discussions

3.1. Restart of crystallization after mesolayers

The nacre within the shells of abalone is mostly composed of tiles of crystalline aragonite that are interleaved

with a 5 wt.% organic matrix in a structure rather crudely described as a "brick and mortar" arrangement [5]. Growth bands, similar to the rings on a tree, which follow seasonal feeding interruptions and separate larger regions of the tiled microstructured nacre, are due to extended interruptions of mineralization [7,8]. The separated sections of inorganic $CaCO_3$ undergo changes in morphology preceding and following growth interruption. In both the flat pearl and trepanning methods the transitory morphologies leading to steady-state tile growth after growth band interruption were observed. Fig. 2a shows an SEM micrograph of a growth band in the fracture surface of an abalone shell. Four regions can be identified: block-like aragonite, an organic region, spherulitic aragonite and finally the steady-state tiled aragonite, as indicated in Fig. 2b and identified by Su et al. [19] through X-ray diffraction. The morphology of the inorganic material created in nucleation is controlled through the interaction of polyanionic proteins [20,21].

The flat pearl and trepanning techniques showed similar results over the course of 6 weeks, indicating that transition from initial mineral nucleation to steady-state mineral growth was not greatly affected by the initial substrate material. This could be due to the thin organic layer which is first blanketed across the potential growth surface, as described by Fritz et al. [17] and Zaremba et al. [22]. The sequential morphologies of this growth sequence are presented in Fig. 3. An initial random nucleation of a precursor mineral phase on the implanted substrates begins after 1 week of growth. As will be discussed later, this layer was identified by Raman spectroscopy as aragonite. As described by Weiner et al. [23], many organisms begin mineralization through amorphous precursor phases.

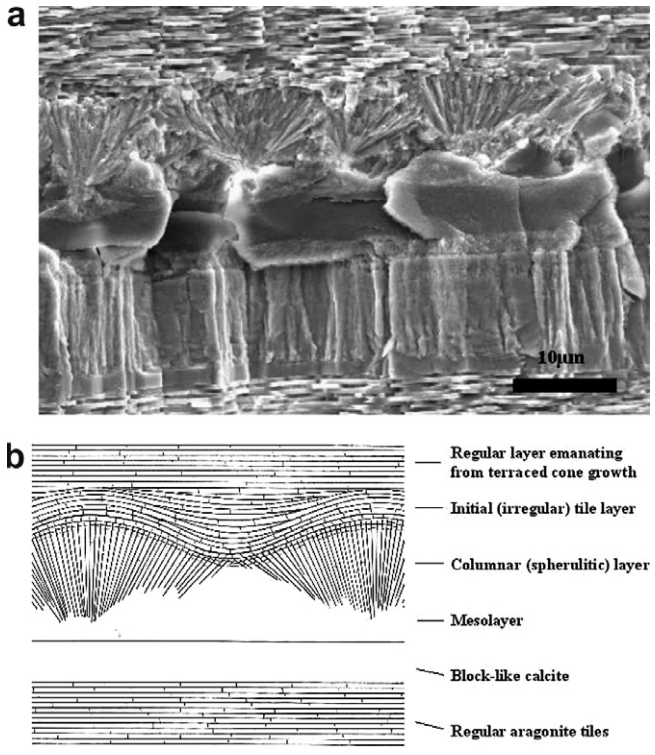

Fig. 2. Cross-sectional view of spherulitic to tile transition after growth interruption: (a) SEM and (b) schematic diagram.

After 2 weeks of implantation, the precursor aragonite has spread across the entire substrate. None of the original implantation is left exposed. Seen in Fig. 3, the morphology of deposited mineral transitions to spherulitic aragonite between the second and third weeks.

After 3 weeks of implantation, the tops of each spherulitic bundle appear flattened. This is thought to be the result of a constant pressure or rubbing force exerted by the mantle of the animal itself. Indeed, it is proposed that the animal forms the structure of the shell through a mechanical–chemical action. The self-assembly of aragonite in nacre does not translate into the overall architecture of the shell; the animal continuously molds it. The animal has the ability to apply a significant amount of binding force to keep itself attached to virtually any surface. This force translates to an approximately equal and opposite force applied normal to the growth surface of the shell. The epithelial layer of the mantle sits directly over the growth surface. As the animal moves along a rock or a wall it twists itself in a rotating manner. The epithelial skin slides back and forth along the shell, producing a sanding effect over the growing mineral structures. This mechanical flattening of the growing surface occurs throughout the nacre deposition region.

After 4 weeks of implantation, the spherulites are fully formed as a result of the divergent growth of aragonite columns along the fast-growing *c*-axis direction. The cross-sectional view of a growth band, shown in Fig. 2, shows the divergent growth of these columns. They spread apart into a lower density as growth continues after 5 weeks of implantation. Between 5 and 6 weeks of implantation the aragonite morphology transforms towards the regular tiled aragonite microstructure, as shown at the top of Fig. 3. It is hypothesized that this transition may occur as the ends of each spherulitic needle become nucleation sites for aragonite tiles. The intermittent deposition of the organic matrix which is believed to inhibit crystal growth [24] molds the spherulitic aragonite needles into an increasingly laminate structure, eventually reaching the steady-state aragonite tile formation. The "Christmas tree"-like growth fields associated with tiled aragonite growth [17,22,26,27] can be seen in Fig. 4. Lin and Meyers [8] observed that the initial spacing of the "Christmas trees" following growth interruption, approximately 4 μm, was smaller than the 10 μm steady-state spacing. This is corroborated by the irregular initial tile formation on top of the spherulitic growth seen in Fig. 2. The first tiles are smaller since they have to conform to a more irregular surface. The spacing in Fig. 4, approximately 4.5 μm, is still lower than the average steady-state 10 μm value.

The first mineral layers formed after 1 week of implantation and were identified by Raman spectroscopy as aragonite. The position of the Raman bands shown in Fig. 5

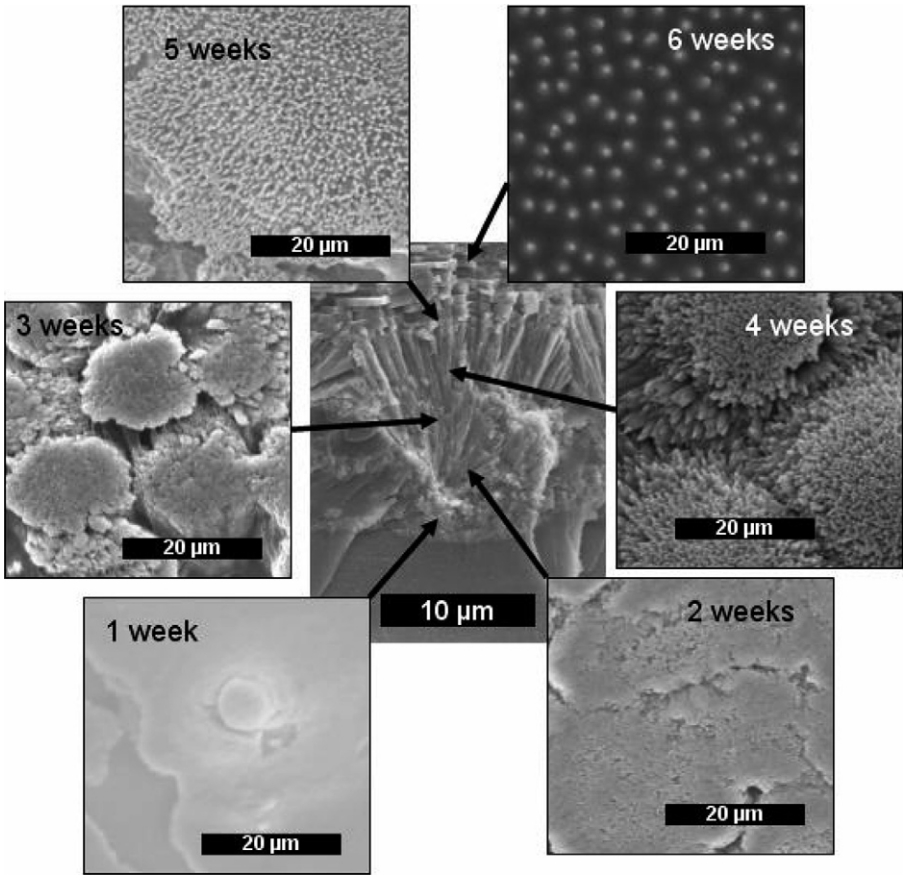

Fig. 3. Summary of sequential growth from flat pearl and trepanning experiments.

coincide with those reported by Urmos et al. [25] for biogenic aragonite. The intense band, near 1086 cm^{-1} (A_{1g}) corresponds to the ν_1 symmetric stretching of the carbonate ion. Further verification was provided through EDS. These results are in concurrence with those described by Su et al. [19].

From the cross-sectional micrograph of a growth band and the data from the sequential growth images, we can

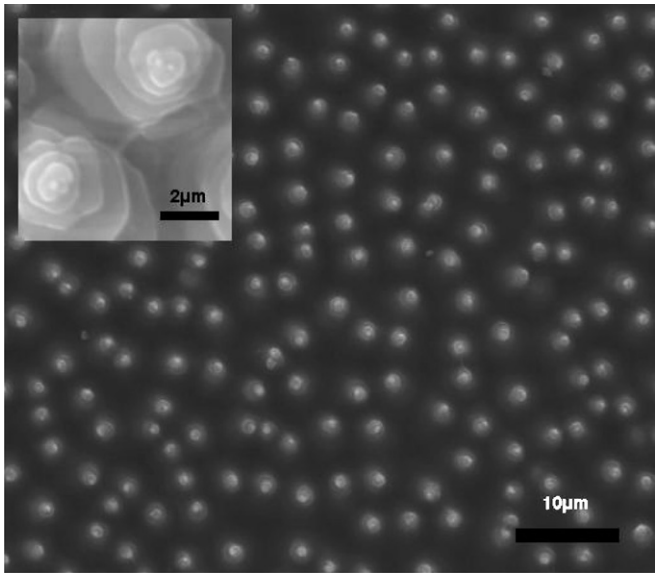

Fig. 4. Tile growth through organic layers on flat pearl 6 weeks after implantation; insert shows detail of the 'terraced growth' (or Christmas tree) pattern.

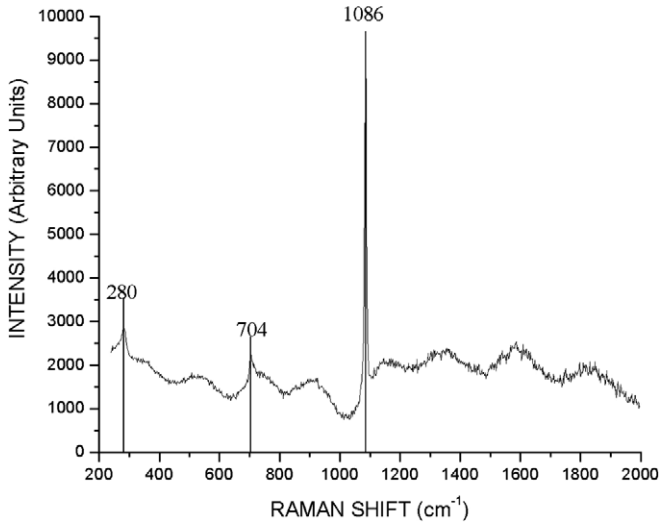

Fig. 5. Raman spectra of implanted flat pearl 1 week after implantation. Raman bands verify the material to be aragonite.

estimate the growth rate of spherulitic aragonite between the third and sixth weeks of implantation. The average height of a spherulite bundle, h, is 10 μm from initiation to tile growth. This growth occurred over a time, t, of 3 weeks. Thus, the average growth rate velocity of the spherulitic calcite, V_G, is:

$$V_G = \frac{h}{t} \quad (1)$$

The growth rate is found to be approximately 0.5 μm per day (5.78×10^{-12} m s^{-1}). These results are comparable to the growth rate previously found through similar observations using the flat pearl technique [8]: (2.3×10^{-11} to 1.5×10^{-10} m s^{-1}).

3.2. Organic membranes

Six weeks after implantation, both the flat pearl and the trepanning experiments showed steady-state growth of hexagonal aragonite tiles. The growth surface exhibited the well-documented "Christmas tree" structure. The process by which this structure is formed has been well described [8,17,28–30], yet remains the subject of some debate. The existence of mineral bridges connecting individual layers was first demonstrated by Schäffer et al. [28] and later confirmed by others [29–31]. These bridges represent the continuation of mineral growth in the c-axis from a preceding layer of tiles; thus, sequential nucleation is not required. They protrude through the growth-arresting layers of proteins, creating sites on the covering organic layer where mineralization can continue. These mineral bridges are the base upon which the next tile forms. The sequence in Fig. 6 shows, in schematic fashion, how tiles are formed one on top of another. Here the growth sequence is as follows: (i) organic scaffolding forms as interlamellar membranes between the layers of tiles arresting c-direction growth; (ii) a new tile begins growth through the porous membrane; (iii) the new tile grows in every direction, but faster along the c-axis; (iv) a new porous organic membrane is deposited, arresting c-axis growth of the new tile while allowing continued a- and b-axis growth, mineral bridges begin to protrude through the second organic membrane while sub-membrane tiles continue to grow along the a- and b-axis. Sub-membrane tiles abut against each other and a third tile begins to grow above the membrane.

A detailed view of mineral bridges enabling growth through a permeable organic membrane is shown in Fig. 7. Holes in the organic nanolayer, which were identified by Schäffer et al. [28], are thought to be the channels through which growth continues. Fig. 7 also shows how mineral growth above the membrane is faster than growth in the membrane holes, because of the increase in contact area with surrounding calcium and carbonate ions. Cartwright et al. [32] described how pore size within the organic matrix could influence the rate of mineral bridge growth. Since these holes are small (30–50 nm diameter), the flow

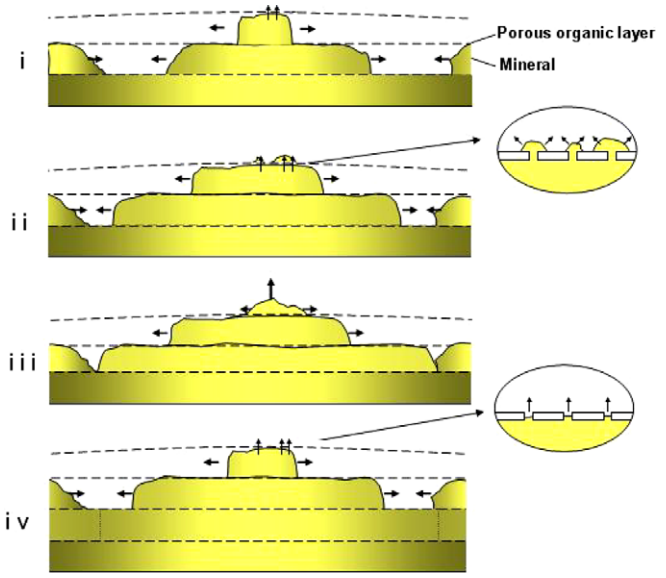

Fig. 6. Schematic representation of the steady-state growth of tiled aragonite within organic scaffolding.

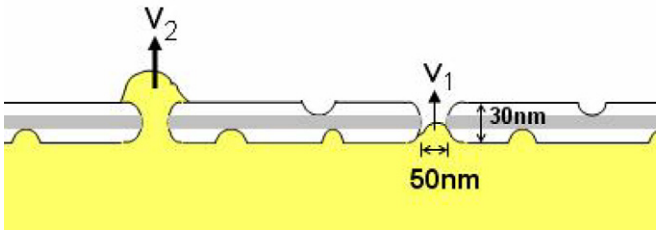

Fig. 7. Detailed view of mineral bridges forming through holes in organic membrane ($V_1 < V_2$).

of ions is more difficult, resulting in a reduction of growth velocity to $V_1 \ll V_2$ (Fig. 7). V_2 is the unimpeded growth velocity in the c-direction. The supply of Ca^{2+} and CO_3^{2-} ions to the growth front is enabled by their flow through the holes in the membranes. This explains why the tiles have a width to thickness ratio of approximately 20, whereas the growth velocity in the orthorhombic c-direction is much higher than in the a- and b-directions.

The specimen surfaces after 6 weeks of implantation (Fig. 8) shows the typical growth morphology characterized by "terraced cones". Unlike previous washed specimens [8], the organic scaffolding between growing tiles (first observed and described by Nakahara et al. [33–35]) can clearly be seen. These sheets of protein form a continuous covering over the entire surface of the shell. If mineral growth was not dependent on the subsurface crystal tiles, aragonite should form randomly across the protein membrane. However, this does not occur. A clear continuity of tiles above and below the membrane can be observed through the cross-sectional view in Fig. 8. The stacks of tiles protrude through the membrane, exposing only the top few layers of aragonite to the calcium-rich epithelial space. Yet all the tiles continue to grow below the membrane, filling in the space along the a and b crystallographic

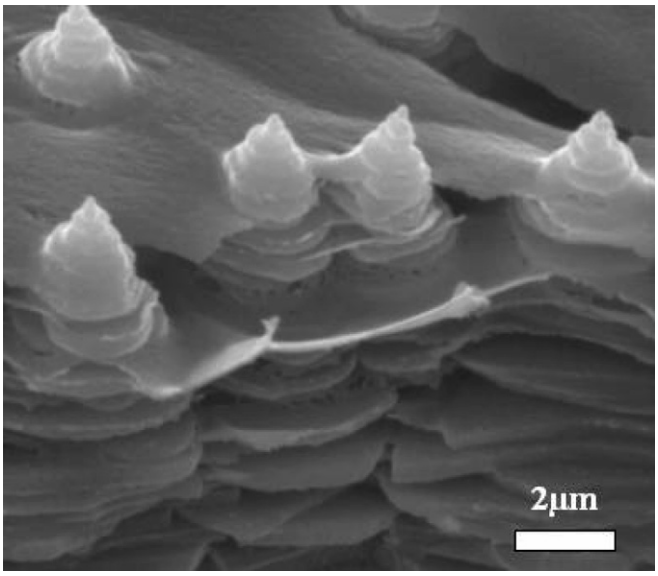

Fig. 8. Side view of intermediate tile growth through organic layers on flat pearl 5 weeks after implantation.

directions. This requires a permeable membrane to allow calcium and carbonate ions to pass through and crystallize on the surfaces below. Holes observed within the membrane both through atomic force microscopy (AFM) and SEM were ~50 nm in diameter; these are more than sufficient for the permeation of the ~1 nm diameter molecules [28]. As small crystal structures protrude through the membrane in the form of mineral bridges, they provide both the site on which subsequent tiles may form as well as a mechanical system binding the layers of tiles together. Fig. 9 provides a schematic diagram of the ion diffusion and aragonite growth processes through these membranes.

3.3. Mineral bridges

Fig. 10 shows fracture surfaces exposed by tension tests with the force application direction parallel to the *c*-axis. Irregular features, the remnants of the organic layer and mineral bridges, can be seen attached to these mineral surfaces of freshly fractured nacre in Fig. 10a. Fig. 10b shows some regions (marked A) containing fabric of the organic layer, where other regions (marked B) are characteristic of the mineral. In order to ascertain that some of these features are indeed mineral bridges, the organic component of the nacre was removed through the hydrazine deproteination process described in Section 2. The fracture surfaces after deproteination are presented in Fig. 10c and d. Transverse to the *a*- and *b*-axes of growth, holes and subsequent mineral bridges cover the (001) planes of the aragonite tiles. These SEM images match what has been observed by AFM by Schäffer et al. [28] and by transmission electron microscopy (TEM) by Song et al. [29,30], Barthelat et al. [31] and Feng et al. [36,37]. Song et al. [29,30] report a higher concentration of mineral bridges around the center than in the outer span of each tile. This may be the result of the growth of each tile beginning from a central expansion along the *a*- and *b*-axes. This process provides the center of each tile a longer period existence, resulting in a higher probability of mineral bridge formation in the middle. These mineral bridges may also play an important role in the mechanical response of the system as described by Song et al. [30] and Meyers et al. [38]. Evans et al. [39] and Wang et al. [40] suggested that the rough nature of tile surface asperities leads to inter-tile friction. They hypothesize that friction is the principal source of shear resistance between tiles. However, there is a significant number of mineral bridges between tile interfaces that were not considered by them. At the onset of plastic deformation, broken mineral bridges may play a role in forming the asperities that subsequently resist shear [38].

Further evidence of these mineral bridges is provided through transmission electron microscopy (TEM). A TEM cross-section perpendicular to the direction of growth is shown in Fig. 11. Interlamellar mineral bridges are indicated by arrows. They are 20–30 nm in height and

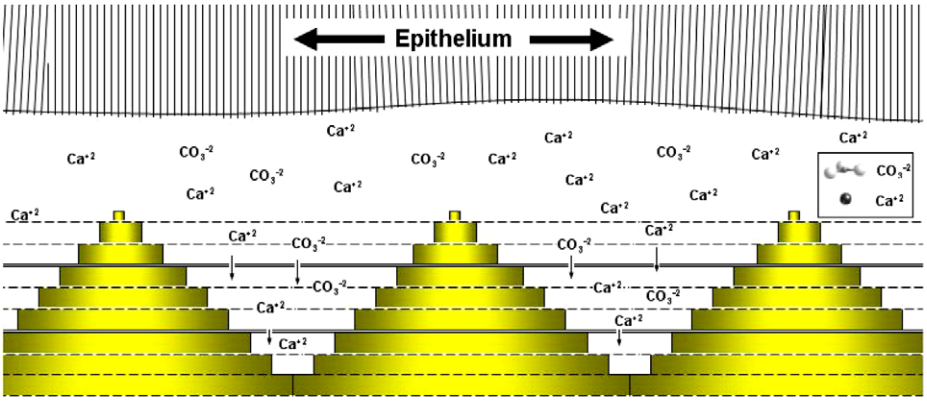

Fig. 9. Schematic representation of Ca^{2+} and CO_3^{2-} ion diffusion through organic scaffolding.

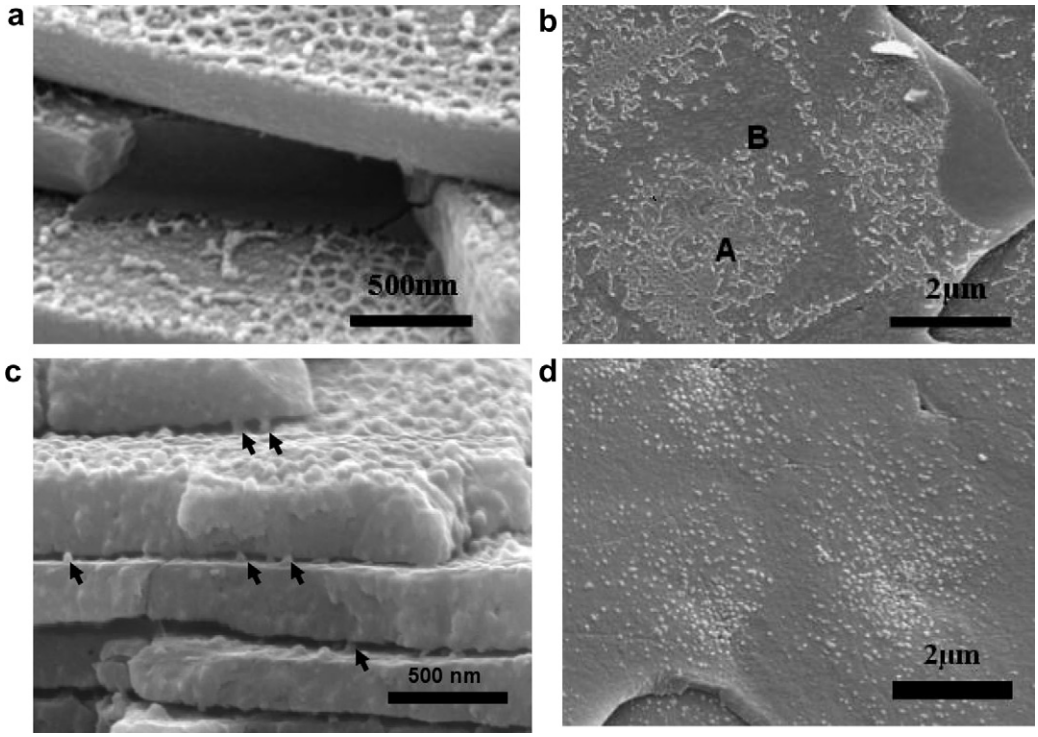

Fig. 10. (a) Interface between tiles (before deproteination) with organic matrix surrounding mineral bridges; (b) tile surface (before deproteination) with regions where organic matrix remains (A) and does not exist (B); (c) mineral bridges (marked by arrows) between aragonite tiles after 9 h of hydrazine deproteination; (d) asperities, many of which are remnants of mineral bridges, concentrated at the center of a aragonite tile after 9 h of hydrazine deproteination.

approximately 50 nm in diameter, confirming previous estimates [28–38].

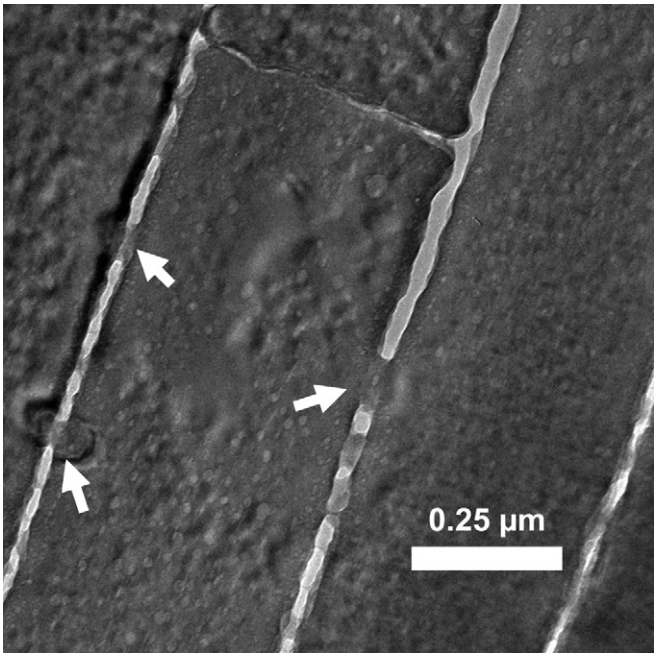

Fig. 11. Transmission electron micrograph of nacre cross-section showing mineral bridges between tile interfaces.

4. Conclusions

A detailed examination of the growth process of abalone nacre was conducted. The flat pearl and trepanning methods were used to observe the sequence of events following interruptions during growth band formation. The results, summarized in Fig. 3, and the observations of fractured surfaces enable the following conclusions:

(a) The process in which crystallization restarts after periods of mesolayer interruption was observed. Both the flat pearl and trepanning technique showed similar results, in which steady-state growth of 10 μm aragonite tiles was achieved after approximately 6 weeks of precursor transitory phases. The majority of the transitory phase occurred in the form of a spherulitic aragonite polymorph, as shown through Raman spectroscopy. The growth rate was estimated to be ~0.5 μm per day, which matches previous findings.
(b) It is proposed that the animal forms the structure of the shell through both mechanical and chemical actions. The self-assembly of aragonite does not translate into the overall architecture of the shell; the animal continuously molds with an applied rubbing force from its mantle.

(c) During steady-state formation of aragonite tiles, an organic scaffolding was observed. Transmembrane mineral growth bridges, approximately 50 nm in diameter and 20–30 nm in height, exist between layers of aragonite tiles.

Acknowledgements

We thank Profs. J. Mckittrick, A. Hodge, and K.S. Vecchio for insightful observations; Ryan Anderson for his assistance at ITL facility at UCSD; and E. Kisfaludy for the laboratory facilities at the Scripps Institution of Oceanography. The assistance provided by Evelyn York with the scanning electron microscopy is greatly acknowledged. We also thank Norman Olson for his assistance at the Cryo-Electron Microscopy Facility at UCSD, which is supported by NIH Grants 1S10RR20016 and GM033050 to Dr. Timothy S. Baker. This research is supported by the National Science Foundation Grant DMR 0510138.

References

[1] Sarikaya M. An introduction to biomimetics: a structural viewpoint. Microsc Res Tech 1994;27:360–75.
[2] Srinivasan AV, Haritos GK, Hedberg FL. Biomimetics: advancing man-made materials through guidance from nature. Appl Mech Rev 1991;44:463.
[3] Mayer G. Rigid biological systems as models for synthetic composites. Science 2005;310:1144–7.
[4] Sanchez C, Arribart H, Giraud-Guille MM. Biomimetism and bioinspiration as tools for the design of innovative materials and systems. Nat Mater 2005;4:277–88.
[5] Currey JD. Mechanical properties of mother of pearl in tension. Proc R Soc Lond B 1997;196:443–63.
[6] Jackson AP, Vincent JFV, Turner RM. The mechanical design of nacre. Proc R Soc Lond B 1988;234:415–40.
[7] Menig R, Meyers MH, Meyers MA, Vecchio KS. Quasi-static and dynamic mechanical response of *Haliotis rufescens* (abalone) shells. Acta Mater 2000;48:2383.
[8] Lin A, Meyers MA. Growth and structure in abalone shell. Mater Sci Eng A 2005;390:27–41.
[9] Lin AYM, Meyers MA, Vecchio KS. Mechanical properties and structure of *Strombus gigas*, *Tridacna gigas*, and *Haliotis rufescens* sea shells: a comparative study. Mater Sci Eng C 2006;26:1380–9.
[10] Sarikaya M, Gunnison KE, Yasrebi M, Aksay JA. Mechanical property–microstructural relationships in abalone shell, vol. 174. Pittsburgh, PA: Materials Research Society; 1990, p. 109–16.
[11] Sarikaya M, Aksay JA. In: Case S, editor. Results and problems in cell differentiation in iopolymers. Amsterdam: Springer-Verlag; 1992. p. 1.
[12] Simkiss K, Wilbur KM. Biomineralization. Academic Press; 1989.
[13] Bauerlein E, editorBiomineralization. Weinheim: Wiley–Intercience; 2000.
[14] Mann S. Biomineralization. Oxford; 2001.
[15] Belcher AM. Spatial and temporal resolution of interfaces, phase transitions and isolation of three families of proteins in calcium carbonate based biocomposite materials. PhD thesis, 1996.
[16] Belcher AM, Wu XH, Christensen RJ, Hansma PK, Stucky GD, Morse DE. Control of crystal phase switching and orientation by soluble mollusk shell proteins. Nature 1996;381:56–8.
[17] Fritz M, Belcher AM, Radmacher M, Walters DA, Hansma PK, Strucky GD, et al. Flat pearls from biofabrication of organized composites on inorganic substrates. Nature 1994;371:49.
[18] Termine JD, Danes ED, Greenfield, Nylen MU. Hydrazine-deproteinated bone mineral. Calc Tissue Int 1973;12:73–90.
[19] Su X, Belcher AM, Zaremba CM, Morse DE, Stucky GD, Heuer AH. Chem Mater 2002;14:3106.
[20] Aizenberg J, Albeck S, Weiner S, Addadi L. Crystal–protein interactions studied by overgrowth of calcite on biogenic skeletal elements. J Cryst Growth 1994;142:156–64.
[21] Touryan LA, Lochhead MJ, Masrquardt BJ, Vogel V. Sequential switch of biomineral crystal morphology using trivalent ions. Nat Mater 2004;3:239–43.
[22] Zaremba CM, Belcher AM, Fritz M, Li Y, Mann S, Hansma PK, et al. Critical transitions in the biofabrication of abalone shells and flat pearls. Chem Mater 1996;8:679–90.
[23] Weiner S, Sagi I, Addadi L. Choosing the crystallization path less traveled. Science 2005;309:1027–8.
[24] Bevelander G, Nakahara H. In: Omori M, Watabe N, editors. The mechanisms of biomineralization in animals and plants. Tokyo: Tokai University Press; 1980. p. 19–27.
[25] Urmos J, Sharma SK, Mackenzie FT. Characterization of some biogenic carbonates with Raman spectroscopy. Am Mineral 1991;76:641–6.
[26] Shen XY, Belcher AM, Hansma PK, Stucky GDS, Morse DE. Molecular cloning and characterization of lustrin A, a matrix protein from the shell and pearl nacre of *Haliotis rufescens*. J Biol Chem 1997;272:32472.
[27] Fritz M, Morse DE. The formation of highly organized biogenic polymer/ceramic composite materials: the high-performance microaluminate of molluscan nacre. Colloid Interf Sci 1998;3:55.
[28] Schäffer TE, Ionescu-Zanetti C, Proksch R, Fritz M, Walters DA, Almqvist N, et al. Does abalone nacre form by heteroepitaxial nucleation or by growth through mineral bridges? Chem Mater 1997;9:1731–40.
[29] Song F, Zhang XH, Bai YL. Microstructure and characteristics in the organic matrix layers of nacre. J Mater Res 2002;17:1567–70.
[30] Song F, Soh AK, Bai YL. Structural and mechanical properties of the organic matrix layers of nacre. Biomaterials 2003;24:3623.
[31] Barthelat F, Li CM, Comi C, Espinosa HD. Mechanical properties of nacre constituents and their impact on mechanical performance. J Mater Res 2006;21:1977–86.
[32] Cartwright JHE, Checa AG. The dynamics of nacre self-assembly. J R Soc Interf 2006. doi:10.1098/rsif.2006.0188, http://dx.doi.org/10.1098/rsif.2006.0188.
[33] Nakahara H, Bevelander G, Kakei M. Electron microscopic and amino acid studies on the outer and inner shell layers of *Haliotis rufescens*. Venus Jpn J Malac 1982;41:33–46.
[34] Nakahara H. Calcification of gastropod nacre. In: Westbroek P, De Jong EW, editors. Biomineralization and biological metal accumulation. Dordrecht: D. Reidel Publishing Company; 1982. p. 225.
[35] Nakahara H. Nacre formation in bivalve and gastropod molluscs. In: Suga S, Nakahara H, editors. Mechanisms and phylogeny of mineralizaion in biological systems. New York: Springer-Verlag; 1991. p. 343.
[36] Feng QL, Li B, Cui Z, Li D. Crystal orientation domains found in the single lamina in nacre of the *Mytilus edulis* shell. J Mater Sci Lett 1999;18:1547–9.
[37] Feng QL, Cui FZ, Pu G, Wang RZ, Li HD. Crystal orientation, toughening mechanisms and a mimic of nacre. Mater Sci Eng C 2000;11:19–25.
[38] Meyers MA, Lin AYM, Chen PY, Muyco J. Mechanical strength of abalone nacre: role of the soft organic layer. J Mech Behav Biol Mater; in press.
[39] Evans AG, Suo Z, Wang RZ, Aksay IA, He MY, Hutchinson JW. Model for the robust mechanical behavior of nacre. J Mater Res Soc 2001;16:2475.
[40] Wang RZ, Suo Z, Evans AG, Yao N, Aksay IA. Deformation mechanism in nacre. J Mater Res Soc 2001;16:2485.